PHYSICAL REVIEW B VOLUME 21, NUMBER 10 15 MAY 1980

Electronic structure of ordered sulfur overlayers on Ni(001)

E. W. Plummer, B. Tonner, and N. Holzwarth
Physics Department and Laboratory for Research on The Structure of Matter, University of Pennsylvania, Philadelphia, Pennsylvania 19104

A. Liebsch
Institut für Festkörperforschung, Kernforschungsanlage Jülich, D-5170 Jülich, Germany
(Received 30 August 1979)

Angle-resolved photoelectron spectroscopy is used to measure the dispersion, linewidth, and photoionization cross section of the electronic valence levels of $p(2\times2)$ and $c(2\times2)$ S overlayers on Ni(001). Polarized light from a synchrotron is used to identify the symmetry of the individual S $3p$ states and to probe their intensity as a function of photon frequency. The data are compared to various theoretical calculations of the energy levels and of the differential cross section for a Ni_5S cluster as well as for ordered S layers on a semi-infinite Ni(001) substrate. The p states of the $c(2\times2)$ structure exhibit about 1.5 eV dispersion with $\vec{k}_{\parallel}$ whose qualitative behavior is well reproduced by the theoretical results using the layer Korringa-Kohn-Rostoker scheme. The measured and calculated p levels of the $p(2\times2)$ structure, on the other hand, show very little dispersion as a result of the relatively large S–S spacing. The observed linewidth of the S levels is considerably larger (1–2 eV) than the calculated single-particle broadening of the $3p$ levels due to hybridization with the Ni sp band (0–1 eV). Lifetime broadening associated with Auger decay appears to be the main origin of the measured linewidth. The photoionization cross section for normal emission from the $p(2\times2)$ structure exhibits a sharp resonance at about 18-eV photon energy which is not present in the case of the $c(2\times2)$ structure. Theoretical analysis of the cross section suggests that this resonance behavior is primarily due to the dominant S p-to-d transition coupled with strong multiple-scattering interferences of the outgoing wave.

I. INTRODUCTION

One of the main motivations for studying surfaces by means of angle-resolved photoemission is to determine the nature of the chemical bond of adsorbed species.[1] In principle, angle-resolved photoelectron spectroscopy can be used to determine both the electronic and geometrical structure of the surface complex, i.e., how and where the foreign species is bonded to the surface. The geometry could be determined by comparing theoretical calculations as a function of the bonding site either to the observed binding energy and dispersion of the adsorbate levels[2] or to the photon energy dependence or angular dependence of the intensity of adsorbate peaks.[3] In the latter case, it is the multiple scattering of the outgoing wave by the atomic environment which leads to geometry-related modulations of the cross section.

Our objective in this work was to apply angle-resolved photoelectron spectroscopy to an atomic adsorption system with a known geometry in order to obtain a detailed picture of the valence-electronic properties of the adsorbate. The geometrical structures of the chalcogens chemisorbed on Ni(001) are well established.[4] The most frequently studied system is ordered oxygen on Ni(001).[5-10] Oxygen adsorption on Ni(001), however, does not seem to be a reproducible process. The reported angle-resolved data are not compatible. Our initial experience with this system was that obtaining a $c(2\times2)$ structure as determined by electron diffraction did not assure that the photoemission spectra would be unique. There must be several surface phases which produce a $c(2\times2)$ diffraction pattern. Analysis of this system is made more complicated due to the accidental overlap of the oxygen-derived levels with the Ni structure near the bottom of the d band and the two-hole state at 6 eV below the Fermi energy.[11] For all of these reasons we have investigated the $c(2\times2)$ and $p(2\times2)$ structures of sulfur adsorbed on Ni(001). Very high exposures or a temperature treatment far above room temperature can create the same problem with $c(2\times2)$ S observed with $c(2\times2)$ O.[6]

Figure 1 shows the real- and momentum-space geometry of the clean Ni(001) surface and of the two sulfur overlayers. The S atoms are located above the fourfold hollow sites with a Ni–S bond length of 2.19 Å, as determined by low-energy electron diffraction[4] (LEED). Both real and reciprocal space unit cells are squares; the S–S spacing of the $c(2\times2)$ [$p(2\times2)$] structure is $\sqrt{2}$ [2] times the Ni–Ni spacing (2.49 Å) of the (001) face. The corresponding surface Brillouin zones (SBZ) are accordingly smaller.

The electronic properties of these overlayer structures can be visualized by starting with a small cluster containing a single S atom above a square of four Ni atoms in the same arrangement as at the surface. Since this molecule has C_{4v} symmetry, the S p states will form two types of

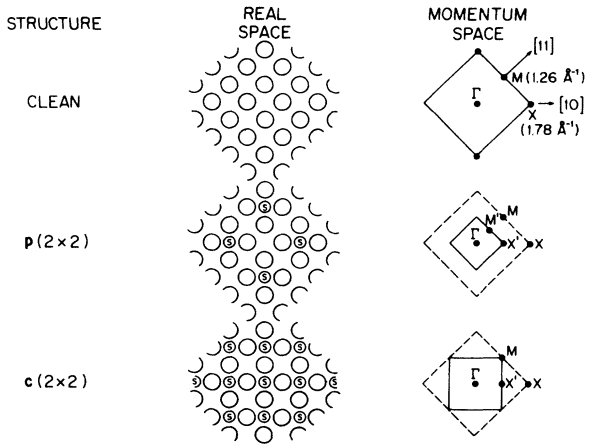

FIG. 1. Real- and momentum-space unit cells of the two ordered sulfur structures $p(2\times2)$ and $c(2\times2)$ on Ni(001). The small circles in the real space representation are the surface Ni atoms.

molecular orbitals with the Ni electrons: a single orbital of a_1 symmetry which is constructed from the S p_z orbital (the z axis specifies the surface normal) and the appropriate symmetric Ni states, and two doubly degenerate orbitals of e symmetry which are derived from the S p_x and p_y levels. When the Ni_4S clusters are placed onto the surface, three basic modifications of these molecular orbitals occur[12]: (i) Due to the direct overlap between S states or due to indirect interaction via the substrate, the p levels form two-dimensional bands; i.e., the energies of the p levels might show a dispersion with $\vec{k}_\parallel$. Obviously, this dispersion reflects the lateral periodicity of the appropriate overlayer SBZ. (ii) As a result of the hybridization of the p orbitals with the continuum of substrate valence states, the sulfur levels may exhibit a finite width. The size of this (single-particle) broadening depends strongly on $\vec{k}_\parallel$ and on the symmetry of the p states. (iii) The symmetry of the bands can not in general be characterized by the symmetry of the initial cluster. Only at Γ and M in the SBZ (see Fig. 1) is it possible to distinguish states of a_1 and e symmetry. At X, the states are characterized by a_1, a_2, b_1, and b_2 symmetry (C_{2v}), whereas along Γ to M or Γ to X only σ and π symmetric states exist (C_{1v}).

We have used angle-resolved photoelectron spectroscopy with the polarized light from a synchrotron to separate and identify the symmetries of the S-derived bands for the two structures shown in Fig. 1. Figure 2 shows a set of characteristic data taken with a photon energy of 21 eV. All spectra are recorded at a fixed value of parallel momentum ($\vec{k}_\parallel = 0.6$ Å^{-1}). This value corresponds to the M' point in the [110] direction (see Fig. 1). Each of

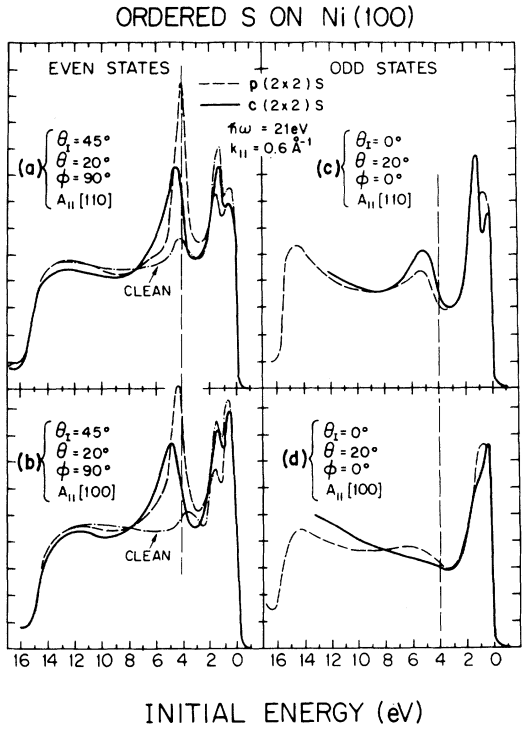

FIG. 2. Characteristic angle-resolved photoelectron spectra for S $p(2\times2)$ and $c(2\times2)$. All curves are at a parallel momentum of 0.6 Å^{-1}. In (a) and (b), only even states can be observed; in (c) and (d), only odd states are excited.

the four sets of curves compares the $p(2\times2)$ spectrum with the corresponding $c(2\times2)$ spectrum. The collection notation is explained in Fig. 3, which shows schematically the angular variables at our disposal. θ_I denotes the angle of incidence of p-polarized light, θ and ϕ are the polar and azimuthal collection angles, and $\vec{A}_\parallel$ denotes the

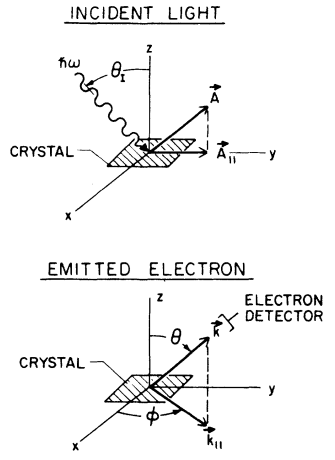

FIG. 3. Schematic drawing of the geometry of angle-resolved photoemission measurements.

orientation of the crystal with respect to the plane of incidence. The binding energy scale for the curves shown in Fig. 2 is given by

$$E_i = \hbar\omega - E_{\text{kin}} - W, \quad (1)$$

where $\hbar\omega$ is the photon energy, E_{kin} is the kinetic energy of the excited electron with respect to the vacuum level, and W is the work function.

The two sets of curves on the left of Fig. 2 are for p-polarized light ($\theta_I = 45°$) with the collection in the plane of incidence ($\phi = 90°$), which is also a mirror plane of the crystal. In this geometry, only states which are even with respect to the mirror plane can be excited. The energy distributions on the right are for s-polarized light ($\theta_I = 0°$) with a collection perpendicular to the electric field ($\phi = 0°$). In this geometry, only states that are odd with respect to the incident mirror plane can be excited. In Figs. 2(a) and 2(c), $\vec{A}_{\parallel}$ lies in the (110) mirror plane, in 2(b) and 2(d) in the (100) mirror plane. The comparison of the S spectra with those for the clean Ni surface in 2(a) and 2(b) (dash-dotted lines) shows that the spectral features between 3 and 7 eV below the Fermi energy are primarily caused by the adsorption of sulfur. The approximately 2 eV wide structure near the Fermi energy is due to the Ni d bands, while the small peak near 4 eV is caused by the top of the sp band. The intensity of these peaks change when S is adsorbed, especially the d-band peak at about 1.7 eV below E_F.

We have systematically investigated the position, shape, and intensity of the S levels as a function of $\vec{k}_{\parallel}$ and photon frequency. We have also performed several theoretical calculations for an Ni_5S molecular cluster and for ordered $c(2\times 2)$ and $p(2\times 2)$ S overlayers on a semi-infinite Ni(001) surface in order to analyze the experimental spectra. The following is the main picture which emerges from this work:

(i) The S p levels of the $c(2\times 2)$ structure show about 1.5 eV dispersion with $\vec{k}_{\parallel}$ whose qualitative behavior is well reproduced by corresponding calculations using the layer Korringa-Kohn-Rostoker (KKR) scheme. On the other hand, both experimental and theoretical results indicate that the p levels of the $p(2\times 2)$ overlayer are nearly $\vec{k}_{\parallel}$ independent as a consequence of the larger spacing between S atoms.

(ii) The experimentally observed width of the S states for both overlayer geometries is significantly larger (1–2 eV) than the calculated single-particle linewidth (0–1 eV). Lifetime broadening appears to be the dominant source of the observed width.

(iii) The cross section for normal emission from the $p(2\times 2)$ structure shows a pronounced resonance at $\hbar\omega = 18$ eV, whereas the $c(2\times 2)$ structure exhibits a much less rapid frequency dependence. The theoretical analysis indicates that the $p(2\times 2)$ resonance is essentially a consequence of the strong atomiclike S p-to-d transition and of constructive multiple-scattering interferences in the outgoing wave. For $c(2\times 2)$, final-state scattering tends to obscure the atomiclike resonant behavior.

(iv) The intensity of the e state for both overlayer structures becomes extremely weak for emission in the (100) mirror plane. This "disappearance" is also found to be a consequence of multiple scattering in the final state.

These experimental and theoretical results illustrate the detailed electronic information which can be obtained with angle-resolved photoemission and tunable synchrotron radiation. The S levels in Figs. 2(a) and 2(b) are considerably more intense and narrow than the peaks seen in the angle-integrated photoelectron spectra from the identical systems.[13] The reason is that in angle-resolved photoemission one can select specific directions and photon energies at which only one peak dominates the spectrum. For example, the very intense peak near 4 eV binding energy in the $p(2\times 2)$ curves of Figs. 2(a) and 2(b) is due to the a_1 symmetric S-derived orbital which is characterized by σ symmetry at this point in the SBZ. The photon energy is chosen to maximize the cross section from this level. Figure 2(c) shows a geometry in which excitation of the σ symmetry state is forbidden: i.e., only the odd p_x, p_y-derived orbital, which has a different energy position and width than the σ state, is observed. The consequence of angle integrating these spectra is a broad asymmetric peak.

II. EXPERIMENTAL PROCEDURE

All of the measurements were made at the 240-MeV storage ring at the Synchrotron Radiation Center of the Physical Sciences Laboratory of the University of Wisconsin. The radiation from the storage ring was dispersed by a 1-m vertically mounted Seya-Namioka monochromator. The photoelectron spectra were measured using a 180° spherical energy analyzer which has an angular acceptance of ±2.5° and which can be moved to any collection angle.[14] The total resolution of the monochromator and analyzer was normally maintained at ~0.3 eV, but could be improved with subsequent loss of signal.

The data were accumulated digitally in a multichannel analyzer. Adsorbate induced peaks in the spectra were visually fitted to Gaussian peak shapes using a digital computer program on a PDP-11. This fitting procedure yielded the area,

position, and width.

The Ni crystal was cleaned by Ar-ion sputtering. The order of the surface was monitored by a 5-keV grazing incidence electron beam. S was adsorbed as H_2S and heated to remove the hydrogen.[15] We observed that a $c(2\times 2)$ diffraction pattern could be formed in at least three ways, producing different photoemission spectra: (i) The adsorbed H_2S could be heated to 200°C, during or after exposure. (ii) The S overlayer could be heated to a higher temperature (300°C). (iii) After repeated exposures of H_2S or before the crystal was completely clean, S could be diffused from the bulk to form a $c(2\times 2)$ pattern. We choose to use treatment (i) since it involves the least amount of heating. The S-derived photoelectron spectra are reproducible using this procedure. To specify this structure further we should have measured the current versus voltage in one or more LEED beams, but we did not have this capability.

The value of $\vec{k}_{\parallel}$ in a spectrum measured at a polar collection angle θ and at a photon energy $\hbar\omega$ is

$$|\vec{k}_{\parallel}|\ (\text{Å}^{-1}) = 0.512(\hbar\omega - E_i - W)^{1/2}\sin\theta\,, \qquad (2)$$

where E_i and W were defined in Eq. (1). Different values of $\vec{k}_{\parallel}$ can be probed by changing either $\hbar\omega$ or θ. We use both of these methods to assure consistency of the data, but whenever possible spectra obtained at photon energies near resonance-line energies will be displayed to facilitate comparison with other data.

Much of the analysis presented in this paper will be based upon simple symmetry selection rules, utilizing polarized light and angle-resolved detection.[7,16] These rules can be easily understood by analyzing the properties of the photoemission matrix element

$$M \propto \langle \psi_f | \vec{A}\cdot\vec{p} | \psi_i \rangle\,, \qquad (3)$$

where ψ_f and ψ_i are the final and initial states of the system, $\vec{p}$ is the momentum operator, and $\vec{A}$ the vector potential. If the collector lies in a mirror plane of the crystal surface, then it can detect only final states which are even with respect to this mirror plane. Odd states have zero amplitude in the mirror plane. The entire matrix element must be even under reflection about the mirror plane; i.e., the symmetry of $\vec{A}\cdot\vec{p}$ dictates the symmetry of the initial state. Thus, by choosing $\vec{A}$ parallel or perpendicular to the collection mirror plane, it is possible to selectively excite even or odd initial states, respectively.

Collection normal to the surface represents a special case because of the higher symmetry at the Γ point. Since initial as well as final states have C_{4v} symmetry for $\vec{k}_{\parallel}=0$, the a_1 and e states can be identified[7] by measuring the dependence of the normal emission signal upon the angle of incidence θ_I. For $\theta_I = 0°$ only the e state can be observed. At an angle of incidence of ~45°, the perpendicular component of the field is maximized[6] and both the a_1 and e states are excited.

III. EXPERIMENTAL RESULTS AND THEORETICAL ANALYSIS

A. Energy levels and dispersion

The binding energy of the a_1 and e symmetry states at Γ can be determined by the procedure outlined above. Figure 4 shows this determination for the $p(2\times 2)$ and $c(2\times 2)$ structures. All four curves are for normal collection. The top curves are for an angle of incidence of 45°. The bottom curves are for $\theta_I = 10°$. We cannot get any closer to $\theta_I = 0°$ with our geometry because the analyzer blocks the incident light. At 21 eV photon energy, calculations show that $|A_\perp/A_\parallel|^2$ has the value 0.04 and 0.8 at $\theta_I = 10°$ and 45°, respectively. Therefore in the $\theta_I = 45°$ spectrum the intensity of the a_1 state relative to that of the e state should be over an order of magnitude larger than in the $\theta_I = 10°$ spectrum.

The $p(2\times 2)$ spectra show that the a_1 state is closer to the Fermi energy than the e state. The measured binding energies of the a_1 and e levels are 4.24 ± 0.05 and 4.9 ± 0.15 eV, respectively, with widths of 1.0 and 2.0 eV, respectively. The shaded portion of the top spectrum shows the e state contribution as determined from computer fitting. Position and width of the e state are obtained from the bottom spectrum in which the a_1 level is not observed. This procedure gives a symmetric a_1

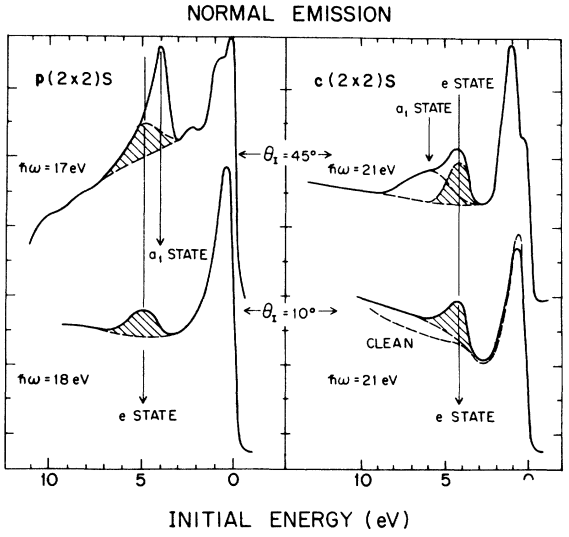

FIG. 4. Normal emission spectra for p-polarized light at two angles of incidence.

state with a width of 1.0 eV [full width at half maximum (FWHM)] in the top spectrum.

The spectra on the right show the same determination for $c(2\times 2)$. Here the a_1 and e states have reversed their order. The a_1 state is at a higher binding energy, 5.86 ± 0.20 eV, with a width of 2.1 eV which is about twice as large as the width of the a_1 state in $p(2\times 2)$. The e state for $c(2\times 2)$ is at 4.44 ± 0.09 eV with a width of 1.35 eV. These results show that there is a large effect on the spectra due to the addition of the extra S atoms necessary to form the $c(2\times 2)$ structure from the $p(2\times 2)$ structure, at least for the states at $\vec{k}_{\parallel}=0$.

The separation of the various S-derived bands at values of $\vec{k}_{\parallel}\neq 0$ is more complicated, especially in a case like that shown in Fig. 4. The binding energies are so close together that they form a single spectral feature. For normal emission, a geometry can be selected ($\theta_I=0°$) where only one state is observed. Its position and width can be determined and subsequently stripped from the spectrum containing both states. At finite $\vec{k}_{\parallel}$, this cannot be done. In each mirror plane the p_x, p_y states split into two bands, one even and the other odd with respect to the reflection about the mirror plane. The p_z state forms an even band which may hybridize with the even p_x, p_y band as a consequence of the interaction with the substrate.[12] Therefore, by using the polarization selection rules described in Sec. II, we can isolate the single odd band in each direction by choosing $\theta_I=0°$ and $\phi=0°$. On the other hand, the two even bands will always appear together in the even collection geometry. Thus we have no way of knowing the energy position or width *a priori* for either of the even bands. There are a few consistency checks dictated by symmetry. For example, the odd and even p_x, p_y-derived bands are degenerate at M in the $c(2\times 2)$ structure.

Figure 5 shows five spectra for $p(2\times 2)$ S taken at different photon energies and collection geometries. The vertical lines show the position of the a_1 and e states at $\vec{k}_{\parallel}=0$. The shaded portions of each spectrum show that a peak of the same position and width as the $\vec{k}_{\parallel}=0$ e state can be fitted to the spectra, leaving a single Gaussian peak at the position and width of the a_1 state at $\vec{k}_{\parallel}=0$. The bottom curve indicates the odd p_x, p_y state at the M' point of the $p(2\times 2)$ SBZ. It has the same position as the e state at Γ within ± 0.1 eV. Only in spectrum (c) can two individual peaks be distinguished in the raw data, but all spectra can be fitted within ± 0.1 eV by peaks given by the normal emission spectra. These two peaks show very little dispersion.

Figure 6 demonstrates that the spectra for the $c(2\times 2)$ structure are not as simple as those for

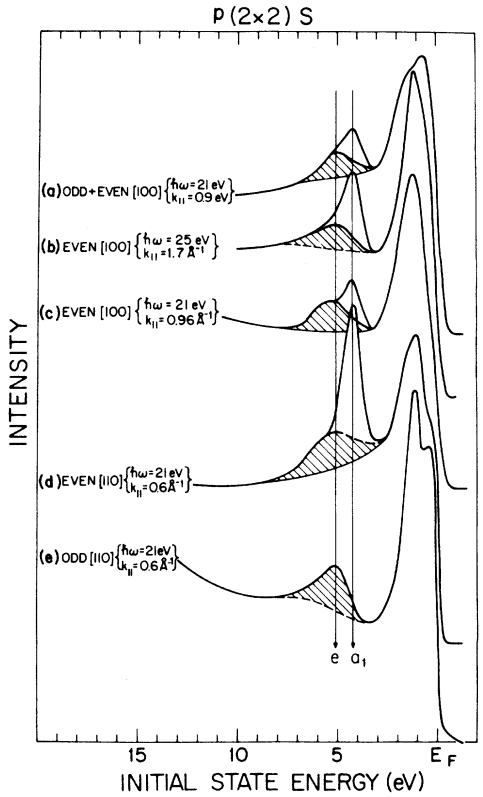

FIG. 5. Photoelectron energy distributions for $p(2\times 2)$. The shaded area of each spectrum shows the contribution from the S e state.

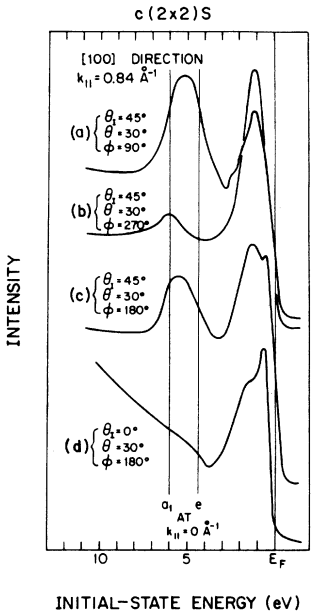

FIG. 6. Photoelectron energy distributions from $c(2\times 2)$ at $\hbar\omega=21$ eV. All curves are for a fixed value of $\vec{k}_{\parallel}$ (0.84 Å^{-1}). The vertical lines indicate the positions of the a_1 and e states at $\vec{k}_{\parallel}=0$ Å^{-1}.

$p(2\times2)$. All four curves are for the same $\vec{k}_{\parallel}$ value near the X' point. The polarization is such that (a) and (b) show only even states, (c) even and odd states, and (d) only odd states. The vertical lines indicate the positions of the a_1 and e levels for $c(2\times2)$ at $\vec{k}_{\parallel}=0$. Clearly, not all spectra in Fig. 6 can be fitted using two Gaussians at these positions. This imples that there must be dispersion. Furthermore, as curve (d) shows, the cross section of the odd state at X' is very small at this photon energy, i.e., its contribution to curve (c) must also be negligible. Thus, the three spectra (a) to (c) consist of two peaks whose relative strength depends on the polarization of the incident light. Their apparent position for one particular polarization can obviously not be directly identified as their binding energy. The importance of this point is illustrated in the spectra (a) and (b). In both cases, emission is in the plane of incidence, in (a), however, away from the incident light direction and in (b) towards it.

Figure 7 shows four examples of our determination of the dispersion of the S energy levels. Panels 7(a) and 7(b) are for $p(2\times2)$ S and panels 7(c) and 7(d) are for $c(2\times2)$ S. Panels 7(b) and 7(d)

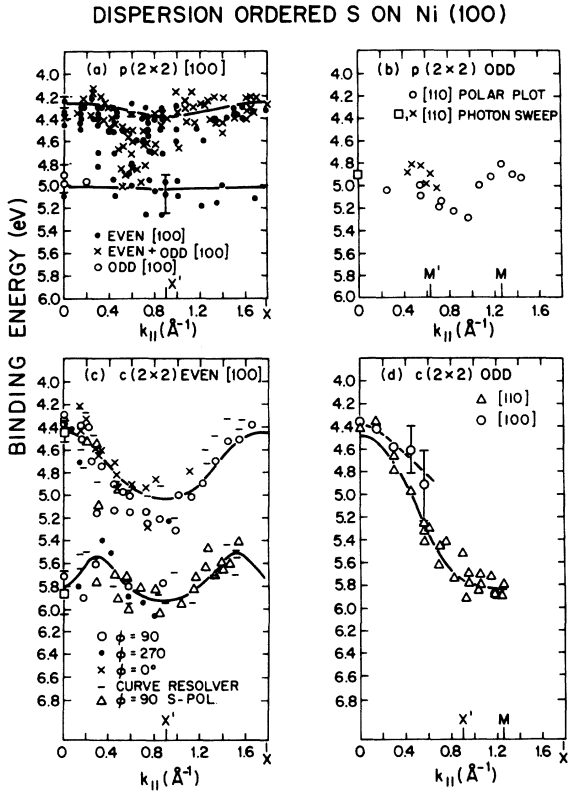

FIG. 7. Measured peak position vs $\vec{k}_{\parallel}$ for $p(2\times2)$ and $c(2\times2)$. The solid lines are the dispersion obtained from curve resolving.

show the measured dispersion of the odd state for $p(2\times2)$ and $c(2\times2)$, respectively. The intensity of the odd band in the [100] direction is very weak for both $p(2\times2)$ and $c(2\times2)$. This has already been illustrated in Figs. 2 and 6. The structure in the $p(2\times2)$ curve in Fig. 2(d) near 6 eV is probably oxygen contamination.[17]

The determination of the dispersion of the two even bands is much more difficult than the determination of the single odd band. Our procedure is to measure the peak position or positions in the raw data as a function of $\vec{k}_{\parallel}$. $\vec{k}_{\parallel}$ is varied by changing both the photon energy and the collection angle [Eq. (2)]. Figure 7(a) shows the raw data for the $p(2\times2)$ even bands in the [100] direction. These data span a photon energy range of 12 to 35 eV, and there are three collection geometries utilized. Since the odd band has no intensity in the [100] direction, all of data should be decomposable into two bands. The solid curves show this decomposition using a curve resolving program on a PDP-11 computer.

The procedure for curve resolving was the following:

(1) The dispersion had to have the periodicity of the overlayer structure (Fig. 1). For example, the dispersion in Fig. 7(a) has to be symmetric about X', so that X is identical to Γ. For example, the energy level positions observed in the second zone of Fig. 7(a) (X' to X) rule out the apparent large dispersion seen in the first zone (0 to X').

(2) The widths of all peaks were assumed to increase monotonically with the binding energy below the Fermi energy, consistent with the measured widths of the odd states. The use of this energy-dependent width will be justified later.

(3) The photon energy, collection angle, and polarization were varied to maximize the intensity of the low-binding-energy narrow peak. (See Fig. 2) The peak position and width of this peak was determined and stripped from other spectra at the same value of $\vec{k}_{\parallel}$.

Figure 7(a) shows that this curve-resolving technique results in little dispersion for $p(2\times2)$ S. Table I lists the measured positions and widths. This table shows that in the [100] direction there is a small dispersion of the p_z band of 0.11 ± 0.08 eV. The largest measurable dispersion for $p(2\times2)$ is shown in Fig. 2, between the [100] and [110] directions. At $\vec{k}_{\parallel}=0.6$ Å^{-1} the energy difference in the p_z band in the two directions is 0.19 ± 0.06 eV. The error bars on the p_x, p_y bands are larger than the measured shifts in peak positions.

In contrast to the $p(2\times2)$ S overlayer the $c(2\times2)$ S overlayer exhibits considerable dispersion as can be seen in Figs. 7(c) and 7(d). The odd p_x, p_y band in the [110] direction disperses by ~1.5 eV

TABLE I. Energies and widths of S($3p$)-derived peaks.

Symmetry	$k_{\parallel}$ (Å^{-1})	Energy (eV)	FWHM (eV)	Energy (eV)	FWHM (eV)
		$p(2\times2)$			
Even	0	4.24±0.05	1.0 ±0.02	4.9 ±0.15	2.0±0.2
Even	[100]				
	0.6	4.35±0.03	1.18±0.03		
	0.89(X')	4.37±0.08	1.2 ±0.1	5.1 ±0.2	
	1.78(X')	4.25±0.06	1.0 ±0.04		
Even	[110]				
	0.63 [M]	4.16±0.03	0.97±0.04	5.2 ±0.2	2.1±0.3
	1.26 [M]	4.18±0.08	1.1 ±0.15		
Odd	0.63 M'			5.1 ±0.2	2.0±0.3
	1.26 M			5.0 ±0.2	2.0±0.2
		$c(2\times2)$			
Even	0	4.44±0.09	1.35±0.13	5.86±0.2	2.1±0.25
	[100]				
	0.3	4.65		5.5 ±0.15	
	0.6	4.90±0.05	1.4 ±0.1	6.0 ±0.15	1.8±0.2
	0.9 [X']	5.0 ±0.15	1.4 ±0.15	5.95±0.15	2.2±0.2
Even	[110]				
	0.6	4.65±0.03	1.26±0.08	5.8 ±0.2	1.8±0.3
	1.26 [M]	4.33±0.05	1.4 ±0.18	6.0 ±0.2	
Odd	[110] 0	4.44±0.09	1.35±0.13		
	0.3	4.75±0.1	1.7 ±0.2		
	0.6	5.4	2.0 ±0.3		
	0.9	5.75±0.15	2.1 ±0.15		
	1.26 [M]	5.85±0.1	2.1 ±0.1		

[Fig. 7(d)]. The two even bands in the [100] direction show dispersion and the appropriate symmetry about the $c(2\times2)$ zone edge at X'.

Figure 8 shows a comparison of the experimental (a) and theoretical (b) dispersion of the S p levels for the $c(2\times2)$ structure along the ΓX and ΓM directions. The solid and dashed lines denote the odd and even sulfur states, respectively. The shaded area in 8(a) indicates the projection of the even Ni sp band. The shaded region in 8(b) shows the approximate (single-particle) broadening of the even p states due to their hybridization with one another and exhibit a rather broad, complicated spectral distribution.[18] The dashed lines in 8(b) indicate only the approximate position of this feature.

The theoretical results are qualitatively similar to those obtained previously for a $c(2\times2)$ oxygen layer on a semi-infinite Ni(001) substrate.[12] The computational procedure is based on the layer-

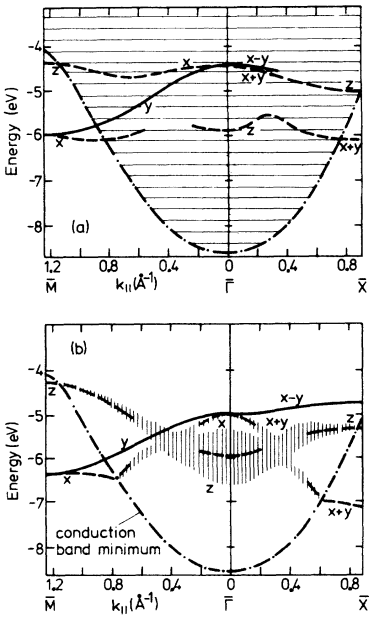

FIG. 8. Comparison of experimental (a) and theoretical (b) dispersion of S levels for $c(2\times2)$. Solid lines: odd p states; dashed lines: even p states. The shaded area in (a) denotes the projection of the even Ni sp band. In (b), the shaded region shows the calculated one-electron width of the p levels.

KKR method. The Wakoh potential is used for the Ni atoms. The S potential is that derived from a self-consistent $X\alpha$ scattered wave calculation for an Ni_5S cluster whose geometry resembles that of the Ni(001) surface.

Since the theoretical results are not fully self-consistent and since they do not include any relaxation shifts, no quantitative agreement with the observed absolute level energies can be expected. The overall trends and the essential qualitative features of the dispersion of the S levels, on the other hand, are reproduced remarkably well. In particular, the reversal of their relative position between the Γ and M points is predicted correctly. At Γ, the p_z level has a higher binding energy than the degenerate p_x, p_y levels. Away from Γ, the two even states hybridize and can be distinguished experimentally only with some difficulty. At M, however, the p states have again pure p_z and p_x, p_y character, the latter two being degenerate on symmetry grounds. Therefore the polarization dependence of these levels allows a clear identification of the observed peak near 6.0 eV as p_x, p_y and of that near 4.3 eV as p_z. This implies that the ordering at M is opposite to that at Γ.

A similar reversal is observed along $\Gamma X'$; however, in this case the experimental assignment is less certain, since the p_x, p_y levels are not degenerate at X' and since the odd p_y state becomes too weak for determination of its precise position. We will return to this "disappearance" of the odd p level in the [100] direction further below and show that this phenomenon is caused by final state multiple-scattering interferences.

The lack of any significant dispersion of the $p(2\times 2)$ sulfur levels suggests that the interaction between p states, either directly or via the substrate, is negligibly small.[19] However, some minor variations of the level energies with emission angle are to be expected even for an isolated adatom on a semi-infinite substrate: Because of the anisotropic environment, the individual Fourier components of the local density of states might have their main weight at slightly different energies. Since the transition matrix element is roughly related to the Fourier transform of the initial state wave function, this anisotropy could lead to an apparent "dispersion." Simple estimates for S on Ni(001) indicate that this effect might be as large as a few tenths of one eV.[20]

A second mechanism which might lead to variations of level energies even for isolated adatoms is the following: If the cross section varies rapidly as function of kinetic energy on a scale given by the intrinsic width of the level, then the line shape will depend on photon energy.[21] As we discuss below, the S $p(2\times 2)$ emission from the p levels shows a reasonantlike frequency dependence with a FWHM of about 4 eV. At photon energies below the resonance maximum, the line shape of the p level will be skewed toward lower binding energies but toward higher binding energies at frequencies above the maximum. This line-shape distortion therefore amounts to an apparent increase in binding energy with increasing photon energy. Realistic estimates based on actual linewidth and frequency dependence of the cross section for the $p(2\times 2)$ structure show that this effect can be of the order of 0.5 eV. Thus the correct lateral periodicity of adatom levels with the overlayer SBZ constitutes a crucial experimental test if dispersion is to be interpreted in terms of the formation of two-dimensional adsorbate-induced bands.

B. Level widths

Table I as well as Figs. 2, 4, 5, and 6 show that there is appreciable broadening of the S $3p$ levels, ranging from a width of less than 1 eV to greater than 2 eV. There are several mechanisms which could be responsible for this width:

(i) hybridization of the S $3p$ levels with the Ni sp band,

(ii) lifetime broadening of the hole state,

(iii) vibrational excitation during ionization, and

(iv) hole localization.

The first mechanism is an initial-state effect caused by the mixing of the two-dimensional S $3p$ levels with the three-dimensional Ni bands. This hybridization can occur at any point in the surface Brillouin zone where there are two-dimensional S states and bulk bands with the same E, $\vec{k}_{\parallel}$, and symmetry. The qualitative variation of this hybridization broadening with E and $\vec{k}_{\parallel}$ can be understood from symmetry arguments. The S $3p$ bands that have odd symmetry in either mirror plane will be discrete, since they cannot hybridize with the even Ni sp band and the Ni odd bands extend only 3 eV below E_F. The even S bands shown by the dashed lines in Fig. 8 will also become discrete bands near the zone boundaries ($\bar{X}$ and $\bar{M}$) where they emerge from the Ni sp band. We have calculated the detailed behavior of the hybridization broadening of the even S $3p$ levels in the $c(2\times 2)$ structure using the procedure outlined in Sec. III A and in Ref. 12. In Fig. 8(b) the center of the S even bands are indicated by the dashed lines while the vertical shading shows the width of the peak. The calculated width is seen to vary greatly with $\vec{k}_{\parallel}$. The largest calculated single-particle width (1 eV) is found for the p_z state at $\vec{k}_{\parallel}=0$, in contrast, the width of the degenerated p_x and p_y states at $\vec{k}_{\parallel}=0$ is zero.

The experimental evidence does not support the

above mechanism for line broadening. The linewidths do not vary with the band symmetry or the value of $\vec{k}_{\parallel}$, instead the width seems to depend only upon the energy of the state below E_F. Figure 9 shows a plot of the measured widths of both $p(2\times 2)$ and $c(2\times 2)$ S from this study as well as S, Se, and Te adsorption data from other work.[22,23] The open circles are for values of $\vec{k}_{\parallel}$ or symmetries where there is no possible mixing of the S states with the Ni bands. Therefore it is clear that hybridization with the *sp* band of Ni does not represent the major contribution to the observed linewidth.

The other three mechanisms listed above are related to the photoexcitation of an electron. The linewidth that results from phonon excitation during the ionization process would correspond to the Frank-Condon envelope that is commonly seen on gas-phase spectra. So far little is known about the magnitude of this effect for atomic species chemisorbed on metallic surfaces. Naively, we would expect the width to be largest for the bonding or antibonding portions of a given band. This would result in a width which was largest at $\bar{\Gamma}$ and $\bar{M}$ and smallest in the center of the zone. This behavior is not observed.

Lifetime broadening due to Auger decay depends roughly on the number of occupied states between a level and the Fermi energy times the number of empty states within the same energy interval above E_F. In general, the level width increases with increasing binding energy. This trend is seen in the data shown in Fig. 9 for the adsorbates as well as for the peaks in the clean Ni spectra due to the *sp* band (dashed line).[24] Neither vibrational not single-particle broadening would exhibit this kind of energy dependence. The preliminary conclusion must therefore be that the observed width is predominantly a consequence of Auger decay of the hole state.

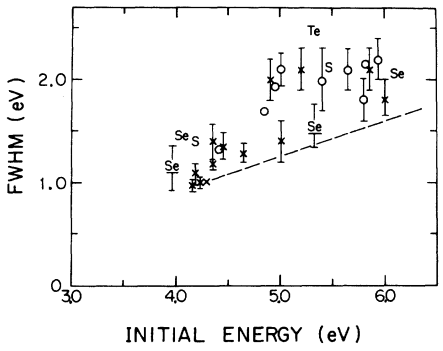

FIG. 9. Measured FWHM of chalcogen derived levels on Ni as a function of binding energy. The symbol Se is from data of Jacobi and Muschwitz (Ref. 22) for Se on Ni(100). The S, Se, Te symbols are data from Capehart and Rhodin on Ni(111) (Ref. 23). The open circles are S data for values of $\vec{k}_{\parallel}$ or symmetries where there is no mixing with the Ni bands.

An additional source of level broadening might be the (partial) localization of the hole state due to many-body interactions. As a result of this effect, $\vec{k}_{\parallel}$ would no longer be a good quantum number and dispersion might, to some extent, be transformed into linewidth. In general, these relaxation processes, as well as the decay of the hole state, constitute some of the self-energy corrections which account for the differences between calculated one-electron energies and measured excitation energies. The data shown in Table I indicate that these corrections for the S $c(2\times 2)$ $3p$ levels depend on $\vec{k}_{\parallel}$, on the binding energy, and on the band index (i.e., the symmetry of the p states).

C. Photoionization cross section

One of the most dramatic effects observed in the photoelectron spectra of $p(2\times 2)$ S is the apparent resonance behavior for emission normal to the surface. Figure 10 shows a series of energy distributions normalized to the incident photon flux.[25] The intensity of the S $3p$ levels becomes very large at a photon energy of about 18 eV. Figure 11 shows plots the frequency dependence of the a_1 and e states. The resonance occurs approximately at 8.5 eV kinetic energy for both states with an FWHM of about 4 eV. Measurements at finite emission angles show a much weaker signal near the resonance energy. At $\hbar\omega = 17$ eV, the FWHM in polar angle for emission perpendicular to the plane of incidence is roughly 20°.[26]

There is also a small enhancement in the secondaries in Fig. 10 at a fixed kinetic energy of approximately 9.2 eV (arrows) which nearly coincides with the kinetic energy (8.5 eV) of the resonance. Andersson[27] has observed a characteristic energy loss in inelastic low-energy electron scattering from S $p(2\times 2)$ at about 18 eV. All of these measurements suggest a high transition probability for this system at excitation energies near 18 eV coupled with a high density of states at about 9 eV above the vacuum level. The second peak at 6.5 eV in the spectrum for $\hbar\omega = 37$ eV in Fig. 10 is primarily due to excitation from the *sp* band.[24]

On the right of Fig. 11, the e-state resonance is shown for nearly s-polarized light. The only difference between this spectrum and the one for p-polarized light (left) is the absence of the peak near 25 eV. This feature is presumably due to the Ni *sp* band which is not excited by s-polarized radiation. Direct transitions from the bulk *sp* states are known to occur at about the same binding energy as the S $3p$ levels for photon energies near 25 eV.[24]

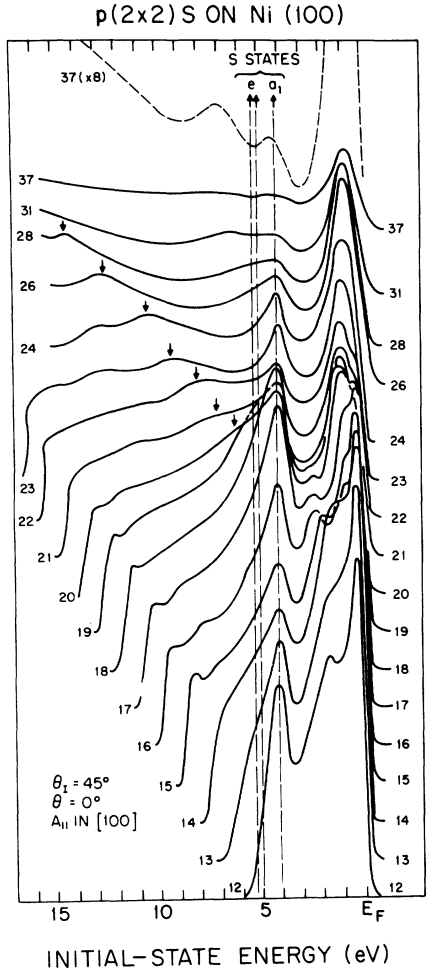

FIG. 10. Normal emission photoelectron spectra of $p(2\times2)$ as a function of photon energy for p-polarized light.

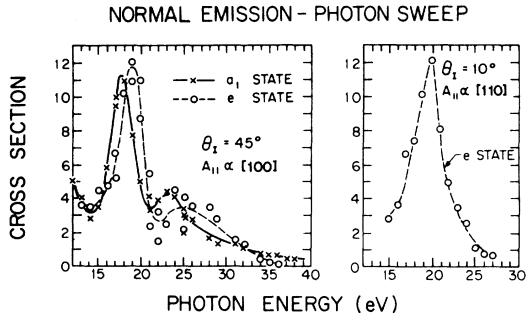

FIG. 11. Photoionization cross section of a_1 and e S states for $p(2\times2)$. Left: curve-resolved a_1- and e-state spectra obtained from the spectra shown in Fig. 10. Right: e-state spectrum at near-normal emission.

Figure 12 shows a comparison of the normal emission ionization cross sections for the $p(2\times2)$ and $c(2\times2)$ S structures. The presence of twice as many sulfur atoms on the surface does not increase the photoionization signal. Also, within experimental error, the $c(2\times2)$ structure does not exhibit any resonancelike behavior.

In order to analyze the origin of the resonantlike emission, we have performed several model calculations. The aim of these calculations was to determine the dominant contributions to the transition matrix element for a reasonable choice of potential parameters rather than trying to obtain a perfect fit of the experimental spectra. In particular, we wanted to determine (a) to what extent the matrix element is influenced by initial-versus final-state effects and (b) how well the electronic excitation is spatially localized at a particular S atom, or, in other words, how important neighboring Ni or S atoms are in an accurate description of initial and final states.

In order to be able to answer these questions we have calculated the differential cross section for an Ni_5S cluster geometry as well as for ordered S $c(2\times2)$ and $p(2\times2)$ layers on a semi-infinite Ni(001) surface. Several qualitative features of the observed variation of the cross section with photon energy and emission angles can be understood on the basis of these models. It should be emphasized, however, that various aspects in these calculations remain somewhat questionable: the non-self-consistent nature of the one-electron potential of the S-Ni system (the same potential is used for initial and final states; posible modifications of ψ_f due to the presence of the hole are ignored), and *ad hoc* treatment of the damping of the outgoing electron via a $\vec{k}$-independent self-energy term, the neglect of relaxation and other self-energy corrections of the hole state (the introduction of a uniform self-energy into the hole propagator does not

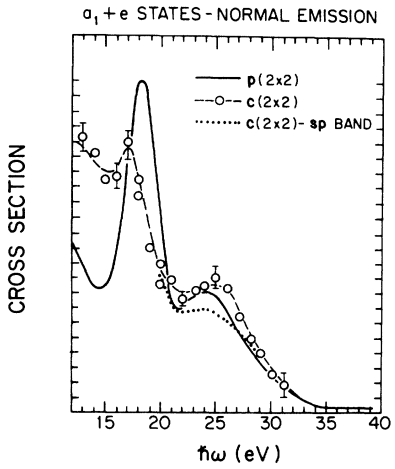

FIG. 12. Photoionization cross section of S a_1 and e states at normal emission for $p(2\times2)$ and $c(2\times2)$.

basically improve the single-particle theory since it only amounts to a Lorentzianlike broadening of spectral features) and, finally, the neglect of microscopic spatial variations of the exciting optical field in the vicinity of the surface. In view of these difficulties, it is clear that our results can only be taken as indicative of some general features of the actual cross section.

Figure 13 shows normal emission distributions for the a_1 and e states of an Ni_5S cluster as a function of the kinetic energy of the outgoing electron (relative to the vacuum level). Since the cluster potential is of the muffin-tin type, we use the $\nabla V \cdot \vec{A}$ form of the matrix element, which can then be written as a sum over the six atomic sites plus a term due to the external region:

$$\langle \psi_f | \vec{\nabla} V \cdot \vec{A} | \psi_i \rangle = \left(\frac{4\pi}{3}\right)^{1/2} \sum_{n=0}^{6} \sum_{m=-1}^{1} Y_{1m}^{*}(\hat{A}) \times \sum_{L_f L_i} (A_{L_f}^{f} R_{l_f l_i} I_{L_f L_i}^{1m} A_{L_i}^{i})_n , \quad (4)$$

where n denotes the site index (the external region has the index o), A_L are the projections of the initial and final states onto the atomic spheres, $R_{l_f l_i}$ denote the radial matrix elements, and I specify the Gaunt integrals which account for the selection rules between the various partial waves $L = (l, m)$.

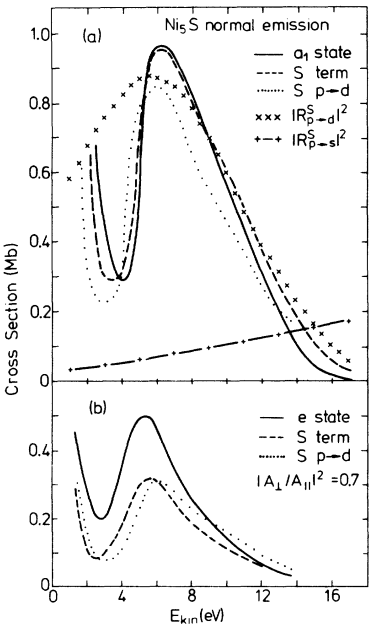

FIG. 13. Ionization cross sections of Ni_5S (a) a_1 and (b) e states at normal emission. Solid lines: actual cross section; dashed lines: cross section if only S contribution to matrix element is retained; dotted lines: cross section obtained from S p-to-d transition. Also shown in (a) are the squares of the S p-to-d and p-to-s radial transition matrix elements.

The differential cross section in units of megabarns (Mb) is then given by the expression

$$\frac{d\sigma}{d\Omega} = 2(10^9 a_0)^2 \frac{\alpha}{\pi} \frac{\kappa}{\hbar\omega} \left| \frac{1}{E_f - E_i} \langle \psi_f | \vec{\nabla} V \cdot \vec{A} | \psi_i \rangle \right|^2 , \quad (5)$$

where α is the fine-structure constant, $E_f = \kappa^2$, and all quantities except the Bohr radius a_0 are measured in atomic units. ψ_f consists asymptotically of an un-normalized outgoing plane wave and various incoming spherical waves.

The electronic states of the Ni_5S cluster are derived using an $X\alpha$-scattered wave scheme in which, after iteration to self-consistency, the Ni potential is replaced by the Wakoh potential which represents a more appropriate choice for the semi-infinite substrate. This S-Ni potential is used in all our calculations for both initial and final state wave functions.

The dashed line in Fig. 13(a) indicates the a_1 cross section if all but the S contribution to the matrix element in Eq. (4) are suppressed. The comparison with the full cross section (solid line) shows that the Ni terms carry rather little weight, since the amplitude of the initial state as well as the transition strength at these sites is relatively small. The S term can be further decomposed into its partial wave components. The main sulfur $p \rightarrow d$ and $p \rightarrow s$ radial matrix elements are also indicated in 13(a). The a_1 cross section is seen to be dominated by the intra-S p-to-d transition which exhibits a maximum at about 6 eV and a Cooper minimum near 21 eV kinetic energy. The detailed shape of the cross section, however, depends strongly on final-state multiple-scattering interferences, as is demonstrated by the dip at 4 eV: The origin of this feature is entirely due to the energy variation of the d_{z^2} projection $A_{L=(2,0)}^{f}(E_f, \vec{k}_f)$ of the outgoing wave onto the S sphere.

Analogous arguments hold true for the corresponding e-state spectra shown in Fig. 13(b). For this state, however, the interferences between the S p-to-d and p-to-s transitions and between S and Ni terms are more pronounced than those for the a_1 state. One reason for this difference is the interesting fact that the intra-S transitions interfere with opposite signs for the a_1 and e states. This point is illustrated by the comparison of the dotted and dashed lines: Whenever the a_1-state emission is enhanced by this interference, that of the e state is reduced and vice versa. (Slight modifications of this rule occur, since the S term involves also weak transitions from s and d states.) This opposite behavior can be easily understood on the basis of selection rules. Keeping only the S p-to-d and

p-to-s transitions in Eq. (3), the matrix elements for the a_1 and e states at normal emission have the form (omitting constant factors):

$$M_a \sim (0.89A_{20}^f R_{p\to d} + A_{00}^f R_{p\to s})A_{10}^i\,, \qquad (6)$$
$$M_e \sim [-\tfrac{1}{2}(0.89A_{20}^f R_{p\to d}) + A_{00}^f R_{p\to s}]A_{1\pm1}^i\,,$$

where explicit numerical values of the Gaunt integrals have been inserted. Apart from the opposite sign in these expressions, the relative weight of the two terms also differs due to the factor $\frac{1}{2}$. Thus the interference with the p-to-s transition has a greater influence on the e-state intensity than that on the intensity of the a_1 state.

These results demonstrate that the relatively broad atomic p-to-d transition for an isolated S atom cannot fully explain the observed resonance behavior. The interaction of the outgoing wave with neighboring Ni and S atoms considerably reduces the width of this transition so that it appears effectively as a rather narrow resonance in the ionization cross section. The comparison of the experimental $c(2\times2)$ and $p(2\times2)$ spectra in Fig. 12 indicates that not only the nearest neighbors of an S atom take part in these multiple-scattering processes but that also more distant S and Ni neighbors must be involved. The effective range of these interferences is essentially determined by the mean free path of the emitted electron.

Figure 14 shows a set of normal emission distributions that illustrate the effect of the extended nature of intial and/or final state on the differential cross section. 14(a) and 14(b) show the emission from the cluster a_1 and e states, respectively, in the case where the final state is derived for an ordered $p(2\times2)$ overlayer on a semi-infinite substrate. 14(c) and 14(d) show the analogous curves for the $c(2\times2)$ structure. Finally, 14(e) and 14(f) show the cross section in the case where both initial and final states are derived for the $c(2\times2)$ overlayer. In each figure part, the full cross section (solid lines) is compared to the sulfur term

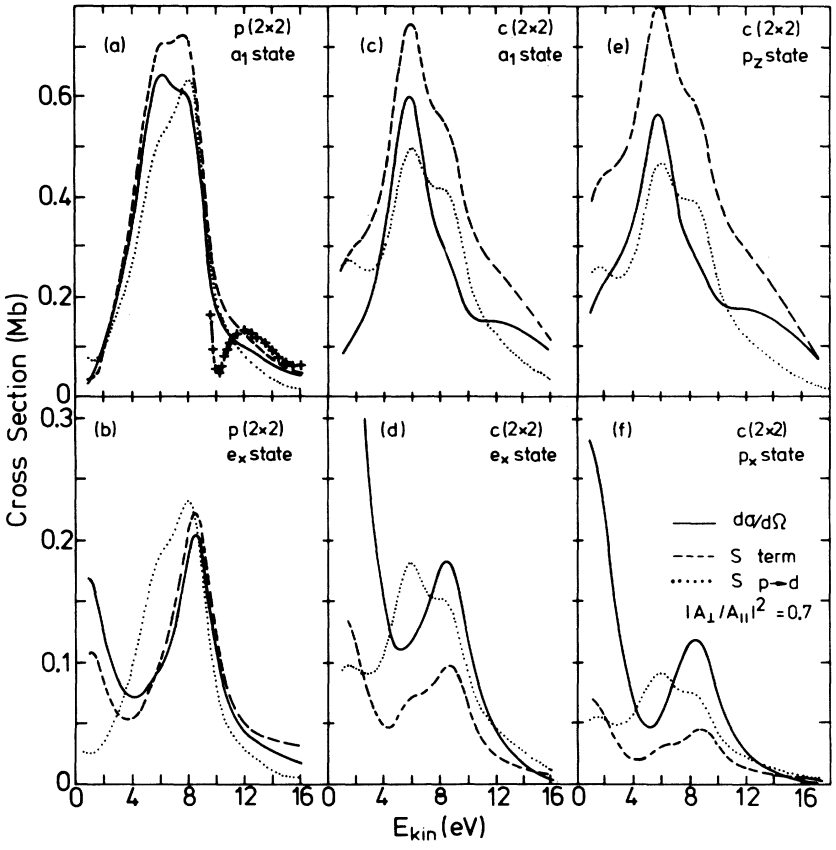

FIG. 14. (a) and (b): normal emission distributions for Ni_5S a_1 and e states, respectively, and $p(2\times2)$ final state. (c) and (d): analogous cross sections for $c(2\times2)$. (e) and (f): p_z and p_x, p_y intensities in the case where both initial and final states are obtained for S $c(2\times2)$ on Ni(001). Solid lines: actual cross section; dashed lines: cross section if only S contribution to matrix element is retained; dotted lines: cross section obtained from S p-to-d transition. Crosses in (a) indicate intensity for small damping (0.02 Ry).

(dashed lines) and to the S p-to-d transition (dotted lines). [In all three cases, the same final state is used; in the latter two, however, only specific contributions to the matrix element in Eq. (3) are retained]. As the mean free path, we have used in all of these calculations the experimentally determined value for clean Ni. It is about 30 Å at 1 eV kinetic energy, drops to approximately 13 Å at 10 eV, and levels off at about 10 Å near 20 eV.

The calculated a_1-state ionization cross sections for $p(2\times 2)$ as well as $c(2\times 2)$ (top row) show relatively narrow resonancelike features at about 6 to 8 eV kinetic energy. In the case of the $c(2\times 2)$ structure, however, the interference between various S partial-wave transitions as well as between S and Ni contributions to the matrix element seem to play a far greater role. Thus, the use of non-self-consistent potentials in our calculations could have a more serious effect on the $c(2\times 2)$ results than on those for $p(2\times 2)$.

Similar results are obtained for the corresponding e-state spectra at the bottom of Fig. 14. As in the case of the Ni_5S cluster, however, the interference between the S $p\rightarrow d$ and $p\rightarrow s$ transitions and between S and Ni terms is much more significant than for the a_1 states. For the $p(2\times 2)$ e state in Fig. 14(b), this effect does not alter the basic resonance behavior; in fact, the e-state resonance is even somewhat sharper than that of the $p(2\times 2)$ a_1 state. In the case of the $c(2\times 2)$ structure, on the other hand, this increased interference nearly obliterates the resonance [see dashed lines in 14(d) and 14(f)].

Obviously, the calculated intensities depend sensivtively on the details of the electronic states which enter the matrix element. For our model, the conclusion seems to be that a fairly pronounced resonance exists for both a_1 and e states of the $p(2\times 2)$ structure, while for the $c(2\times 2)$ overlayer only the a_1 state exhibits a resonancelike cross section. Unfortunately, the large intrinsic peak width of the $c(2\times 2)$ S a_1 and e states does not allow a complete experimental separation at normal emission. A composite spectrum consisting of both a_1 and e states would in our model exhibit three peaks, since the maxima of the individual cross sections do not occur at the same energy. The relative weight of the a_1- and e-state cross sections depends largely on the angle of incidence. In fact, the ratio of their intensities is given by

$$\sigma_{a_1}/\sigma_e \sim |A_\perp/A_\parallel|^2 . \qquad (7)$$

For the results shown in Figs. 13 and 14, the ratio on the right-hand side has the value 0.7 which corresponds to an incidence angle of about 45°. For smaller θ_I, the weight of the a_1 state relative to that of the e state becomes accordingly smaller.

Thus, while we cannot give a quantitative interpretation of the data, the results of our calculations seem at least to give the correct tendency for the $p(2\times 2)$ and $c(2\times 2)$ ionization cross sections. Two aspects which do not appear to be consistent with the measured spectra are (i) the fact that the larger amount of S in the $c(2\times 2)$ overlayer does not increase the signal [Figs. 14(a)–14(d) show intensities per Ni_5S cluster] and (ii) the existence of the observed $p(2\times 2)$ resonance only at relatively small polar angles (FWMH $\approx 20°$). In our results, the resonance intensity decreases far more slowly as a function of polar angle. Both failures could be related to uncertainties regarding the electronic damping in the final state. For longer mean free paths, the upper part of the $p(2\times 2)$ a_1-state resonance near 8 eV [Fig. 14(a)] becomes very intense and narrow, but only so at small polar angles. The crosses in Fig. 14(a) indicate the increase in the amount of finite structure for a self-energy of $\Gamma = 0.02$ Ry. An additional source of discrepancies between theoretical and experimental spectra might be the use of a neutral S potential in the evaluation of ψ_f. The presence of the hole could modify this potential and lead to a lowering and

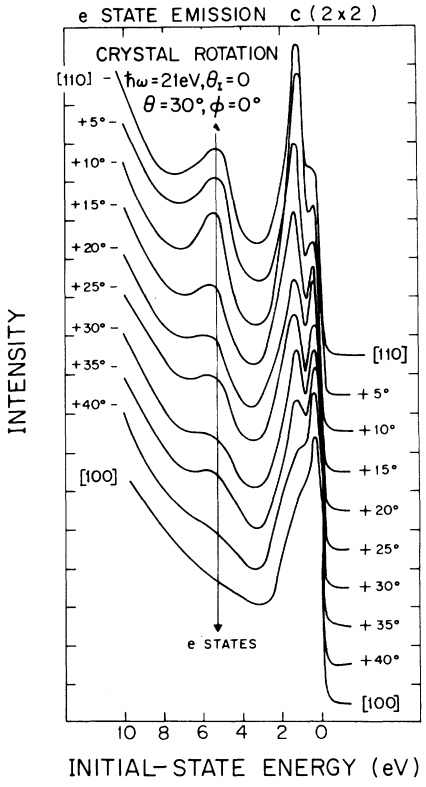

FIG. 15. e-state emission for $c(2\times 2)$ in odd collection geometry at a fixed polar angle. The crystal is rotated about the surface normal between the [110] and [100] azimuths.

narrowing of the S d resonance. A simultaneous change in the interference between the $p \rightarrow d$ and $p \rightarrow s$ transitions could also influence the cross section.

We conclude the discussion of photoionization cross section by considering the weak intensity of the odd state in the [100] direction compared to the [110] direction. This behavior for $p(2\times2)$ and $c(2\times2)$ overlayers was shown in Figs. 2(b) and 6. In Fig. 15 we show a crystal rotation measurement for $c(2\times2)$ S at a polar angle of 30° ($\vec{k}_{\parallel} = 0.85$ Å^{-1}). The light is s polarized with the polarization vector perpendicular to the collection direction. Two observations are worth noting. First, the intensity in the [100] direction is nearly zero, much weaker than in the [110] direction. Second, when the collection is not in a mirror plane the symmetry rules break down. Therefore between the [100] and [110] direction we could have observed three energy levels. This would result in a shift in the peak position, which is not observed.

The intensity variation can be explained theoretically. Figure 16 shows the calculated e-state ionization cross sections for $p(2\times2)$ (a) and $c(2\times2)$ (b) at finite emission angles ($\theta_e = 30°$) along the (110) azimuth (solid lines) and along the (100) azimuth (dashed lines). In the latter case, the intensity is extremely weak and nearly featureless.

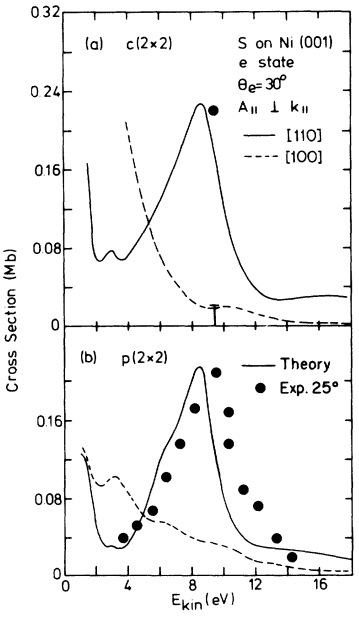

FIG. 16. e-state ionization cross section at $\theta_e = 30°$ for $c(2\times2)$ (a) and $p(2\times2)$ (b) along [110] azimuth (solid lines) and [100] azimuth (dashed lines). Experimental data in (b) are for a collection angle of 25°. The cross section of the experimental data in (a) is divided by two compared to (b) because the calculation does not account for the increased coverage.

Analysis of the contributions to the matrix element suggests that this effect is mainly caused by multiple-scattering interferences which reduce the S d components in the outgoing wave. Thus the curious "disappearance" of the e state in Fig. 15 for emission in the (100) plane seems to be also, like the resonance behavior at normal emission, associated with pronounced single-particle interactions in the final state. The solid circles in Fig. 16(b) show experimental data for the photon energy dependence of the e state in the [110] direction. The two data points in Fig. 16(a) show the intensity difference of this state in the [110] and [100] directions for $c(2\times2)$ S.

IV. CONCLUSION

It has been demonstrated that angle-resolved photoemission is capable of providing a detailed picture of the electronic structure of chemisorbed overlayers. The tunability of synchrotron radiation and its high degree of polarization have been shown to be particularly useful for the analysis of complex adsorbate-induced spectral features. The electronic properties of the two S structures, $c(2\times2)$ and $p(2\times2)$ on Ni(001), have been found to exhibit important differences, both with regard to the energy and momentum distribution of the S $3p$ levels and with regard to the photon energy dependence of their cross section. As we have shown, the main aspects of these observations can be understood with the aid of realistic calculations.

While the primary aim of this work was the analysis of the S-induced states, it is clear from the experimental spectra shown in Fig. 2 that the S adsorption also causes significant changes in the energy region of the Ni d band. These changes depend on $\vec{k}_{\parallel}$ as well as on the polarization of the light; i.e., they are not caused by inelastic scattering of the excited electron.[28] This behavior is in striking contrast to the weak influence on the Ni d-band emission due to adsorption of H.[29,30] The adsorption of H on Ni is believed to proceed mainly via bonding to the Ni $4s$ band.[31] It is tempting therefore to associate the observed d-band changes in the case of S with a chemisorption bond that involves primarily Ni $3d$ rather than $4s$ states. This interpretation, however, would certainly be oversimplified, since *intensity* changes in the d-band region are not related in any direct manner to charge redistributions on the surface Ni atoms.

In particular, it is not possible to determine from the experimental spectra alone to what extent weight of d states has been shifted to the S bonding levels. Our theoretical calculations indicate that the S orbitals have considerable $3d$ as well as $4s$ character within the Ni muffin-tin spheres. Be-

cause of the delocalized nature of the 4*s* electrons, they form the dominant contribution in the interstitial region between S and Ni spheres. Thus, qualitatively we conclude from our results that both Ni 4*s* and 3*d* states contribute to the S bonds. This conclusion differs from theoretical results obtained for small S-Ni clusters using the generalized valence bond scheme.[32] These calculations suggest that the 4*s* electrons dominate the bonding since the 3*d* orbitals are only weakly affected by the S adsorption because of their small radial extent. However, even in these calculations, S states were found to have up to 15% *d* character on the Ni sites.

The major difference between the $c(2\times2)$ and $p(2\times2)$ S overlayers is the amount of dispersion of the 3*p* levels. The energy levels of $p(2\times2)$ S show very little variation with $\vec{k}_{\parallel}$, while the overall bandwidth of the $c(2\times2)$ levels is approximately 1.5 eV. Since the dispersion of the chemisorbed $c(2\times2)$ S levels is about the same as that for a free S layer with the same lateral structure, the dispersion is predominantly a consequence of the direct S–S interaction. The average energy of the $c(2\times2)$ p_z band is 5.35 eV, which corresponds to a 1-eV larger binding energy than in the case of $p(2\times2)$. The average energy of the p_x, p_y states, on the other hand, is about the same for both overlayer geometries (4.9 eV). Overall, the binding energy per S electron is 4.7 eV for $p(2\times2)$ and 5.1 eV for $c(2\times2)$. An interesting observation is the fact that the vibrational properties of the two S overlayers on Ni(001) are very similar[33] despite the pronounced differences in their electronic structure.

It has been proposed by Hagstrom[5,34] and by Fisher[35] that the chalcogens adsorbed in the $c(2\times2)$ configuration on Ni(001) are bonded to two Ni atoms rather than four. The adsorption geometry is the same as shown in Fig. 1, but the bond axes of two adjacent S atoms are perpendicular. Such a structure would have $p(2\times2)$ symmetry with two S atoms per unit cell, leading to a $p(2\times2)$ Brillouin zone containing six S bands instead of three. However, there would exist a degenerate structure with all bound axes rotated by 90°. Both structures would strongly interact with the result that the overall symmetry is still $c(2\times2)$. The observed dispersion shown in Figs. 7 and 8 for half-monolayer coverage is clearly consistent with $c(2\times2)$ symmetry. This result also agrees with LEED diffraction patterns which show an overlayer structure of pure $c(2\times2)$ symmetry.

ACKNOWLEDGMENTS

This work was supported by the National Science Foundation through the Materials Research Laboratory Program under Grant No. DMR-76-80994. The University of Wisconsin Synchrotron Radiation Center is supported by NSF Grant No. 74-15098. We would like to thank S. Weeks, G. Loubriel, and T. Gustafsson for assistance in accumulating data for this paper.

[1] E. W. Plummer and T. Gustafsson, Science 198, 165 (1978); T. Gustafsson and E. W. Plummer, in *Photoemission from Surfaces*, edited by B. Feuerbacher, B. Fitton, and R. F. Willis (Wiley, London, 1977), Chap. 12.

[2] P. K. Larsen, N. V. Smith, M. Schlüter, H. H. Farrell, K. M. Ho, and M. L. Cohen, Phys. Rev. B 17, 2612 (1978); S. Louie, Phys. Rev. Lett. 42, 476 (1979).

[3] A. Liebsch, Phys. Rev. Lett. 32, 1203 (1974); Phys. Rev. B 13, 544 (1976).

[4] See, e.g., J. E. Demuth, D. W. Jepsen, and P. M. Marcus, Phys. Rev. Lett. 31, 540 (1973).

[5] H. D. Hagstrum and G. E. Becker, Surf. Sci. 30, 505 (1972); G. E. Becker and H. D. Hagstrum, Phys. Rev. Lett. 22, 1054 (1969).

[6] S. P. Weeks and E. W. Plummer, Solid State Commun. 21, 695 (1977).

[7] K. Jacobi, M. Scheffler, K. Kambe, and F. Forstmann, Solid State Commun. 22, 17 (1977).

[8] C. Guillot, Y. Ballu, J. Paigne, J. Leconte, P. Thiry, R. Pinchaux, and Y. Petroff, in *Proceedings of the 3rd International Conference on Solid Surfaces, Vienna, 1977*, edited by R. Dobrozemsky, F. Rüdenauer, F. P. Viehbock, and A. Breth (F. Berger and Söhne, Vienna, 1977), p. 1159.

[9] R. J. Smith and G. J. Lapeyre (private communication).

[10] D. Jepsen, C. Noguera, D. Spanjaard, C. Guillot, Y. Ballu, and P. Thiry, Solid State Commun. 28, 741 (1978).

[11] C. Guillot, Y. Ballu, J. Paigne, J. Leconte, K. P. Jain, P. Thiry, R. Pinchaux, Y. Petroff, and L. M. Falicov, Phys. Rev. Lett. 39, 1632 (1977).

[12] A. Liebsch, Phys. Rev. B 17, 1653 (1978).

[13] H. D. Hagstrum and G. E. Becker, Proc. R. Soc. London A331, 395 (1972).

[14] C. L. Allyn, T. Gustafsson, and E. W. Plummer, Rev. Sci. Instrum. 49, 1197 (1978).

[15] $p(2\times2)$ S was formed by exposure to H_2S and subsequent heating to 200 °C.

[16] J. Hermanson, Solid State Commun. 22, 9 (1977).

[17] The intensity of this 6-eV peak is not reproducible and it has the characteristic photon energy dependence of oxygen.

[18] For a detailed plot of the *p*-wave projections of the local density of states in the analogous case of $c(2\times2)$ O on Ni(001) see Fig. 7 in Ref. 12.

[19] Although we have not calculated the dispersion for the $p(2\times2)$ overlayer structure, it clearly would be very small. For a $p(2\times2)$ oxygen monolayer, the calculated overall bandwidth is only about 0.1 to 0.2 eV.

[20]G. Zwicknagl and A. Liebsch (unpublished).
[21]A. Liebsch and E. W. Plummer, Faraday Discuss. Chem. Soc. 58, 19 (1974).
[22]K. Jacobi and C. V. Muschwitz, Solid State Commun. 26, 477 (1978).
[23]T. W. Capehart and T. N. Rhodin (unpublished); Surf. Sci. 82, 367 (1979).
[24]W. Eberhardt and E. W. Plummer, Phys. Rev. B 20, 1444 (1979).
[25]The beam intensity was monitored with an Al_2O_3 NBS calibrated diode, a W mesh, and the Ni normal emission secondaries (see also Ref. 26).
[26]The details of the angular distribution and the monochromator calibration will be published elsewhere.
[27]S. Andersson, private communication.
[28]The arguments against inelastic scattering are presented in more detail in a paper about surface states on Ni(100), E. W. Plummer and W. Eberhardt, Phys. Rev. B 20, 1444 (1979).
[29]F. J. Himpsel, J. A. Knapp, and D. E. Eastman, Phys. Rev. B 19, 2872 (1979).
[30]H adsorption on Ni(100) at room temperature causes similar changes to those observed for Ni(111) (Ref. 29).
[31]T. H. Upton and W. A. Goddard, III, Phys. Rev. Lett. 42, 472 (1979).
[32]S. P. Walch and W. A. Goddard, III, Solid State Commun. 23, 907 (1977); Surf. Sci. 72, 645 (1978).
[33]S. Andersson, Surf. Sci. 79, 385 (1979).
[34]H. D. Hagstrum and G. E. Becker, J. Chem. Phys. 54, 1015 (1971).
[35]G. B. Fisher, Surf. Sci. 62, 31 (1977).